Reaction Chemistry & Engineering

The Development of a Continuous Synthesis for Carbamazepine using Validated In-line Raman Spectroscopy and Kinetic Modelling for Disturbance Simulation

Journal:	*Reaction Chemistry & Engineering*
Manuscript ID	RE-ART-11-2022-000476.R2
Article Type:	Paper
Date Submitted by the Author:	17-Jan-2023

Complete List of Authors:	Glace, Matthew; FDA Wu, Wei; FDA Kraus, Harrison; FDA Acevedo, David; FDA Roper, Thomas; Virginia Commonwealth University, Chemical and Life Science Engineering; Virginia Commonwealth University, Chemical and Life Science Engineering Mohammad, Adil; FDA, Division of Product Quality Research

SCHOLARONE™
Manuscripts

The Development of a Continuous Synthesis for Carbamazepine using Validated In-line Raman Spectroscopy and Kinetic Modelling for Disturbance Simulation

Matthew Glace[1], Wei Wu[1], Harrison Kraus[1], David Acevedo[2], Thomas D. Roper[3] and Adil Mohammad[1*]

[1] Division of Product Quality Research, Office of Testing and Research Office of Pharmaceutical Quality, Center for Drug Evaluation and Research, Food and Drug Administration, 10903 New Hampshire Ave., Silver Spring, MD 20993

[2] Division of Pharmaceutical Manufacturing Assessment I, Office of Pharmaceutical Manufacturing Assessment, Office of Pharmaceutical Quality, Center for Drug Evaluation and Research, Food and Drug Administration, 10903 New Hampshire Ave., Silver Spring, MD 20993

[3] Department of Chemical and Life Sciences Engineering, Virginia Commonwealth University, Richmond, VA 23284

Corresponding author:

* Adil Mohammad
Email: adil.mohammad@fda.hhs.gov

This article reflects the views of the author. It should not be construed to represent FDA's views or policies.

Abstract

Mitigation of failure modes in continuous synthesis (CS) of drug substance (DS) has the potential to widen the adoption of continuous manufacturing (CM) technologies by the

pharmaceutical industry. This work demonstrates the development of a robust continuous process for the synthesis of carbamazepine (CBZ), an essential medicine as per World Health Organization (WHO), facilitated by kinetic modelling and monitored by in-line Raman spectroscopy. Accurate kinetic modelling and the use of validated process analytical technology (PAT) models for quantitative measurement was found to play an important role to develop CS for drug substance. Kinetic data for the formation of CBZ from iminostilbene (ISB) was collected by batch reaction sampling and high-performance liquid chromatography (HPLC) analysis. A non-linear solver and iterative method were applied to determine two sets of Arrhenius parameters simultaneously for the reaction system by minimizing the standard error of model fit. The start-up and dynamic equilibrium stages for the CS of CBZ using continuous stirred tank reactor (CSTR) was modelled based on the batch kinetic data and employed to optimize conversion and simulate process disturbances. An in-line Raman spectroscopy method was successfully developed, validated, and integrated to determine the concentrations of CBZ and ISB within the operating range for the CS. The CS kinetic model was evaluated experimentally from startup to dynamic equilibrium over 10 residence times with monitoring by HPLC and in-line Raman spectroscopy. The developed kinetic model in tandem with the in-line Raman successfully predicted the disturbances due to changes in process variables and can serve as useful tools in future design of advanced process control strategies for continuous synthesis of CBZ.

Introduction

The adoption of advanced manufacturing technologies, such as continuous manufacturing (CM), within the pharmaceutical industry has been rising steadily [1-3]. The benefits of transitioning from traditional batch manufacturing to CM include smaller equipment footprint, increased throughput, reduced processing time per unit dose, and agile response time for production during unexpected spikes in demand such as a public health emergency. Advanced manufacturing technologies such as CM can also help improving domestic manufacturing capabilities, thus alleviating to some degree the constraints from global supply chains [4]. Currently, batch manufacturing is still the most widely utilized production method by the pharmaceutical industry. The transition from batch to CM in the pharmaceutical industry is in its early stage and therefore presents unique challenges [2, 5].

With the rising interest in the adoption of CM in pharmaceutical industry, the continuous synthesis (CS) of drug substance (DS) has also been increasing and can be an alternative means to batch synthesis and purification [6-13]. Quality by design, digital twin, and adaptive process control strategies are some examples in the development of CS within the pharmaceutical manufacturing. In 2021, Arden et al. [14] elaborates that while adaptive, model-based controllers should be the next frontier within the pharmaceutical manufacturing sector, several fundamental areas to enable such platforms are lagging other industries. Specifically, in-line process analytical technologies (PAT), which gather process information, are still maturing. PATs are typically used for process monitoring but can also be applied for disturbance diversion and process control [1, 11, 15]. Accurate kinetic models for CS can help to determine how the variation of measurable process parameters and corrective actions may impact product quality. Kinetic modelling for CS of API has

been utilized for optimization and disturbance studies [6, 16]. These works have included the development of a virtual multi-stage CSTR process to predict the impact of disturbances on critical quality attributes[16]. Kinetic modelling of CS can be useful for the management of process disturbances as encouraged by the International Council of Harmonization guidance Q13[3]. The combined use of both validated PAT methods and kinetic modelling to predict and monitor CS of API is seldom reported. The predictive capacity provided by the kinetic model as well as the real-time data provided by the PAT method can be beneficial throughout many stages of process development.

In this work carbamazepine (CBZ) was selected as a model drug product to explore CS process and to test the use of a validated PAT method. In addition to being designated a WHO essential medicine, CBZ is a good model drug for CS due to challenges stemming from relatively low solubility of precursor and reagents as well as polymorphism [17-19]. Although CBZ has been synthesized and recrystallized continuously, no PAT methods have been developed for the synthesis stage[20-23]. Both Raman spectroscopy and focused beam reflectance measurement (FBRM) have been utilized for monitoring CBZ concentration during crystallization[20, 22]. In the current study, the formation of CBZ from iminostilbene (ISB) and an alkali metal cyanate in acetic acid solvent was first synthesized in batch to gather information on the reaction kinetics. A continuous stirred tank reactor (CSTR) model was employed to optimize reaction conditions and simulate dynamic process conditions. A HPLC method and a quantitative in-line Raman spectroscopy method were both developed and validated. CBZ was synthesized in high yield using a single-stage CSTR. In-line Raman spectroscopy and HPLC monitoring verified the kinetic

model for the predicted optimal conditions. Several process disturbances were also simulated and demonstrated experimentally.

Materials and Methods

Materials

All chemicals were used as received from vendors. Iminostilbene (ISB) was procured from Biosynth Carbosynth (San Diego, CA). Glacial acetic acid and potassium cyanate (KOCN) were procured from Sigma Aldrich (St. Louis, MO). Optima acetonitrile was procured from Fisher Chemical (Fair Lawn, NJ). CBZ was procured from Ria International (East Hanover, NJ). Milli-Q® water was produced in-house via a Milli-Q® Direct 8 water filtration system (EMD Millipore; Burlington, MA). HPLC reference standards for Carbamazepine, Iminostilbene, and 10,11-Dihydro-5H-dibenz[b,f]azepine-5-carboxamide were procedure from USP (Rockville, MD).

Batch Chemistry Procedure

A 250 mL, 3-neck borosilicate round bottom flask (RBF) was charged with 96 mL glacial acetic acid, 600.0 mg iminostilbene (ISB, 3.10 mmol, 1.00 eq.) and a magnetic stir bar. All connections were lubricated with Dow-Corning (Midland, MI) high vacuum grease. The RBF was placed under a reflux condenser, a Chemglass (Vineland, NJ) PTFE thermocouple, and a glass stopper. The RBF was attached to a Chemglass AREX-6 Digital Pro Heating Magnetic Stirrer attached to the temperature probe. The system was heated to thermal equilibrium at the desired temperature with magnetic stirring at 500 RPM. A mass of 277.0 mg potassium cyanate (KOCN, 3.41 mmol, 1.10 eq) was dissolved to a final volume of 4.00 mL in Milli-Q H_2O (18 MΩ·cm @ 25 °C) to final concentration of

0.854 M. The 0.854 M KOCN solution was injected into the heated RBF, marking T = 0 for reaction sampling. HPLC timepoint samples were prepared by pipetting 200 µL of crude reaction mixture to a final volume of 3 mL in HPLC grade acetonitrile (15x dilution) followed by secondary dilution within the HPLC calibration range (5-100 ppm). Reaction aliquots were collected for T = 0.5 min, 1 min, 2 min, 3 min, 5 min, 10 min, 15 min, 30 min, 45 min, 1 hour, 1.5 hours and 2 hours. The reaction procedure was repeated for 30°C, 40°C, 45°C, 50°C, 60°C, and 70°C.

Continuous Synthesis (CS) Procedure

For the CSTR system, a 400 mL vessel in the Mettler Toledo (Columbus, OH) EasyMax 402 reactor system was charged with 144 mL glacial acetic acid and 6 mL water. The CSTR was heated to 61 °C with water as the cooling medium and the overhead stirrer (4-prong, upward, 35 mm, 15° pitch) was maintained at 500 rpm. The Tornado (Mississauga, ON) Spectroscopy system (HyperFlux Pro Plus 785) and Marqmetrix (Seattle, WA) immersion probe (PN: WP-785-RP-VF) was utilized in the CSTR to monitor CBZ and ISB concentrations. Clear stock solutions of ISB in glacial acetic acid and KOCN in Milli-Q H_2O were prepared at 6 mg/mL and 500 mg/mL respectively. Three Masterflex (Gelsenkirchen, Germany) peristaltic pumps (Model no. 77301-44, 07522-20) were calibrated and used with size 14 or 16 precision silicon tubing platinum for material transfer. The outlet tubing height was positioned to maintain the CSTR level at 150 mL, and the outlet material was collected for HPLC sampling periodically. The inlet concentration flow rates were set at 2.4 mL/min and 0.1 mL/min for the ISB and KOCN stocks, respectively, to achieve a 1-hour mean residence time. A process flow diagram

of the continuous process and a photograph of the experimental apparatus is shown in Figure 1A and 1B, respectively.

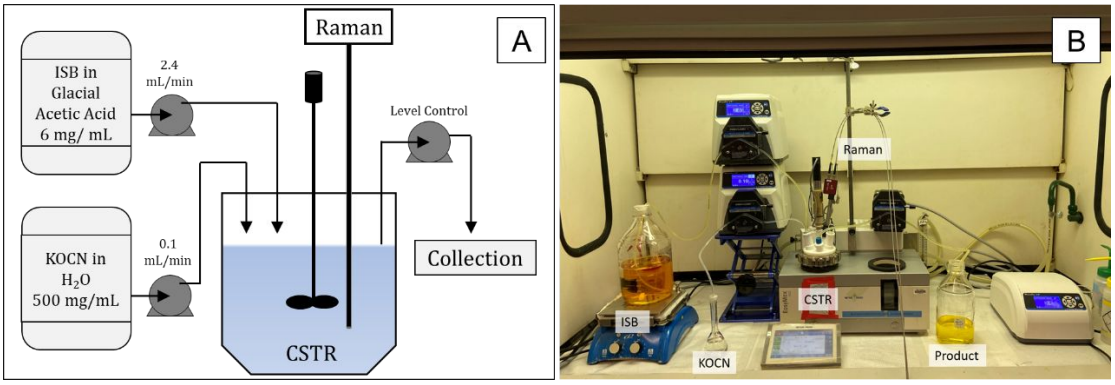

Figure 1: CSTR process flow diagram under normal operating condition (A) process flow diagram and (B) experimental setup

High Performance Liquid Chromatography (HPLC)

The Agilent (Santa Clara, CA) HPLC (1260 infinity) was the basis for all analysis including the in-line Raman spectroscopy method. The HPLC method was validated according to the principles of ICH Q2 (R1) [24] , USP General Chapter 1225 [25], and USP General Chapter 621[26]. For concentration analysis of carbamazepine, iminostilbene (Impurity B) and carbamazepine related compound A (10,11-Dihydro-5H-dibenz[b,f]azepine-5-carboxamide, CBZ-A), a 6-point calibration curve was prepared from USP standards in the range of 5 -100 parts per million (ppm).. The stability of the instrument was assessed by six system suitability injections and the accuracy of the calibration curve was assessed by five quality control samples at each of four concentration levels for each analyte. The method repeatability, method robustness and sample stability were assessed prior to data analysis.

In-line Raman Spectroscopy monitoring

A quantitative in-line Raman spectroscopy model was developed for the measurement of CBZ and ISB concentrations within the ranges and conditions of the continuous synthesis process. Calibration curves, system suitability, and quality control samples were prepared by dissolving CBZ and ISB together in a solution of 96:4 acetic acid to H_2O (volume basis). The accuracy and precision of this method was demonstrated over three days of method validation and during intermediate-term repeatability studies. Raman spectra were collected with a Tornado spectral system and Marqmetrix in-line immersion probe with an 800-millisecond exposure time and 300 scans averaged per spectra. Each spectra took four minutes to collect, and a two-minute pause was implemented between spectra. Samples were equilibrated to 61 °C in an EasyMax reaction vessel with overhead stirring at 200 rpm prior to spectra collection. For each day of method validation, the concentration of the prepared samples and the general collection procedure is outlined in the supplementary information. The accuracy and precision (relative standard deviation) of the quality controls and system suitability were assessed during the method validation. For each validation period, the concentrations of CBZ and ISB were input into the Raman calibration model as determined by off-line HPLC analysis.

The in-line Raman model development was performed in Python. Throughout most of the spectrum, CBZ and ISB showed significant overlap with each other and interference from the background. Given the challenging spectral features, a Python function was scripted to rapidly assess the feasibility of thousands of potential peaks for high correlation to each substrate concentration by ordinary least squares regression. After subtracting the average of the ten blank spectra, the modelling function established a linear baseline

matrix as a function of wavenumber in the designated interval (Start: Stop) on the sample spectra (eq. 1).

1) $$\text{Baseline} = \frac{\text{Spectra Count}_{\text{Stop}} - \text{Spectra Count}_{\text{Start}}}{\text{Wavenumber}_{\text{Stop}} - \text{Wavenumber}_{\text{Start}}} \text{ x } (\text{Wavenumber} - \text{Wavenumber}_{\text{Stop}}) + \text{ Spectra Count}_{\text{Start}}$$

Trapezoidal approximation was applied to integrate the area between the spectra and linear baseline of length 'n' to return a singular value (eq. 2).

2) $$\text{Area} = \sum_{i=0}^{n-1} \{(\text{Spectra Count}_i + \text{Spectra Count}_{i+1})/(\text{Baseline}_i + \text{Basline}_{i+1})\}/2$$

After the area was established for each sample in the calibration curve dataset, a 1st order linear regression by least sum of squares correlated the calculated area to the concentration data and calculated root mean squared error (RMSE) of the fit. The area calculation and linear regression was iterated over thousands of potential baselines and the models with the lowest RMSE were returned for both CBZ and ISB. A robust calibration peak throughout the method validation period was selected for each species.

Kinetic Modelling

The reaction mechanism incorporated in the batch kinetic model includes an instantaneous equilibrium and two simultaneous reactions as shown in equations 3-5. The reactive isocyanic acid (HOCN) formed from the reversible protonation of potassium cyanate (KOCN) with acetic acid [27]. The pKa for acetic acid is 4.75 and for the isocyanic acid is 3.7 (eq 3, 6). CBZ formed from the reaction between ISB and HOCN following the 1st order reaction mechanism proposed by Tiwari et. al [28] (eq. 4). Isocyanic acid may irreversibly decompose under acidic conditions to form carbon dioxide and ammonium ions [27] (eq. 5).

3) $$KOCN + CH_3COOH \leftrightarrow HOCN + CH_3COOK$$

4) $$ISB + HOCN \rightarrow CBZ$$

5) $$HOCN + H_3O^+ \rightarrow CO_2 + NH_4$$

HOCN is assumed to be in instantaneous equilibrium with KOCN for this model. With the dilute reaction conditions employed, it can be inferred that $[H_3O^+]$ is constant and the degradation of the cyanate follows first order with respect to HOCN only (eq. 6).

$$6)\quad [\mathrm{HOCN}] = \frac{[\mathrm{KOCN}]}{\frac{3.7}{[\mathrm{H}^+]} + 1}$$

For computational efficiency, the potassium cyanate concentration is reduced by the two reactions directly although in reality it is the isocyanic acid that is being consumed. Because the potassium cyanate and isocyanic acid are in an instantaneous equilibrium, this implementation is mathematically equivalent. The pre-exponential factors A_1 and A_2 and the activation energies $E_{A,1}$ and $E_{A,2}$ are the Arrhenius parameters that correspond to the CBZ formation and cyanate degradation respectively. For notation, 't' represents time (sec) and 'T' represents temperature (Kelvin). The reaction rate for each of the three substrates at any given time (t) are defined in equations 7-9. Note that these equations 7-9 apply only to the batch reaction, where the reaction rate of each component is equal to its respective time derivative of concentration.

$$7)\quad \frac{\mathrm{d}[\mathrm{CBZ}]}{\mathrm{dt}} = \mathrm{A}_1\, \mathrm{e}^{\frac{-\mathrm{E}_{\mathrm{A},1}}{8.314 \times \mathrm{T}}} [\mathrm{ISB}]\, [\mathrm{HOCN}]$$

$$8)\quad \frac{\mathrm{d}[\mathrm{ISB}]}{\mathrm{dt}} = -\mathrm{A}_1\, \mathrm{e}^{\frac{-\mathrm{E}_{\mathrm{A},1}}{8.314 \times \mathrm{T}}} [\mathrm{ISB}]\, [\mathrm{HOCN}]$$

$$9)\quad \frac{\mathrm{d}[\mathrm{KOCN}]}{\mathrm{dt}} = -\mathrm{A}_1\, \mathrm{e}^{\frac{-\mathrm{E}_{\mathrm{A},1}}{8.314 \times \mathrm{T}}} [\mathrm{ISB}]\, [\mathrm{HOCN}] - \mathrm{A}_2\, \mathrm{e}^{\frac{-\mathrm{E}_{\mathrm{A},2}}{8.314 \times \mathrm{T}}} [\mathrm{HOCN}]$$

The standard error (S.E.) is defined in eq. 10 for the purpose of fitting the Arrhenius parameters to the HPLC dataset. The model has four degrees of freedom (df) corresponding to the four fitted Arrhenius parameters.

$$10)\ \mathrm{S.E.} = \sqrt{\frac{\sum_{n=1}^{n} \sum_{t=1}^{t} \left\{ \mathrm{CBZ}_{t,T}^{\mathrm{Model}} - \mathrm{CBZ}_{t,T}^{\mathrm{HPLC}} \right\}^2}{\mathrm{df}}}$$

The standard error of the fitted iterative kinetic model to the acquired HPLC timepoints was defined as a function in Python [29]. The packages NumPy [30], pandas [31] and SciPy [32] were installed and utilized. The equations were approximated by numerical discretization

utilizing the backwards difference scheme. After convergence testing, a timestep (Δt) of 0.1 seconds was implemented for the iterative numerical approximation. The SciPy algorithms 'basinhopping' and 'minimize' were used to simultaneously optimize the four Arrhenius parameters. The starting ISB and KOCN concentrations were modelled as prepared. The package Matplotlib was used to generate plots [33].

For the continuous process modelling, inlet and outlet terms for each species are defined and implemented in eq. 11-13. The inlet term is dependent upon inlet concentrations (designated by subscript '*inlet*') and flow rates (U). For the typical startup procedure, the initial concentrations of each species will be zero. Effective process control is assumed such that the outlet flowrate is the sum of the inlet flow rates of the ISB stream (U_1) and the cyanate stream (U_2) and the filled volume of CSTR-1 is constant (V). Perfect mixing is also assumed for the CS modelling. The discretized form of the batch and continuous equations is reported in the supplementary information.

11) $$\frac{\mathrm{d[CBZ]}}{\mathrm{dt}} = \mathrm{A_1\, e^{\frac{-E_{A,1}}{8.314 \times T}}\,[ISB]\,[HOCN] - \frac{[U_1 + U_2][CBZ]}{V}}$$

12) $$\frac{\mathrm{d[ISB]}}{\mathrm{dt}} = -\mathrm{A_1\, e^{\frac{-E_{A,1}}{8.314 \times T}}\,[ISB]\,[HOCN] + \frac{[U_1][ISB_{inlet}]}{V} - \frac{[U_1 + U_2][ISB]}{V}}$$

13) $$\frac{\mathrm{d[KOCN]}}{\mathrm{dt}} = -\mathrm{A_1\, e^{\frac{-E_{A,1}}{8.314 \times T}}\,[ISB]\,[HOCN] - A_2\, e^{\frac{-E_{A,2}}{8.314 \times T}}[HOCN] + \frac{[U_2][KOCN_{inlet}]}{V} - \frac{[U_1 + U_2][KOCN]}{V}}$$

To improve the speed and accuracy of the solver and facilitate convergence, intermediate fitting parameters (P_1:P_4) were established as a function of each Arrhenius parameter (Eq. 14 -17). These fitting parameters were adjusted directly by the optimization algorithm.

14) $P_1 = 10^{A,1}$

15) $P_2 = 10^{A,2}$

16) $P_3 = 10^4 \cdot E_{A,1}$

17) $P_4 = 10^4 \cdot E_{A,2}$

Results and Discussion

Reaction Route

Proper chemistry selection during the batch development stage is critical to achieving a viable CS process. Insolubility of reagents, slow kinetics or multiple incompatible stages can make CS difficult or impossible. Numerous reaction routes for the carbamoylation of CBZ or CBZ derivatives have been reported before [34-41]. An alkali cyanate reagent route outlined in Figure 2 was selected for the development of a CS process for CBZ because it is a single stage reaction, has favorable kinetics, and is safer and environmentally friendly as compared to more toxic reagents such as chlorosulfonyl isocyanate [39] or phosgene [40] used in other routes.

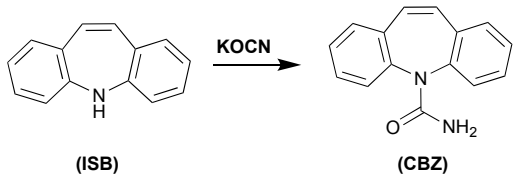

Figure 2: Carbamoylation of 5H-Dibenz[b,f]azepine (ISB) to form 5H-dibenzo[b,f]azepine-5-carboxamide (CBZ).

A variety of N-substituted ureas have been synthesized using alkali cyanates and catalytic acids [28]. Alkali cyanates have previously been utilized in the batch synthesis of CBZ [37] and similar benzodiazepine derivatives [34, 35, 38]. Acetic acid as a reaction solvent and catalyst was investigated following the process of Eckhardt [37]. To avoid precipitation issues in CM, stock concentrations were diluted to room temperature solubility.

Batch Reaction

The batch reaction proceeded with viable kinetics at moderate temperature and using reasonable equivalents of the alkali cyanate. The SciPy ‘basinhopping’ algorithm in Python was globally convergent at multi-parameter optimization in the reaction design

space. The convergence was demonstrated by a final solution that was independent of the initial input values. The SciPy function 'minimize' and 'BFGS' scheme was used to generate the covariance matrix. The correlation of the fitting parameters is reported in Table 1. Note that the fittings parameters are an intermediate to the Arrhenius parameters and described in eq. 14-17. Broadly, some collinearity persisted between the predicted pre-exponential factors (A_1 and A_2) and activation energies ($E_{A,1}$ and $E_{A,2}$) that was unable to be fully mitigated using this optimization scheme. The predicted value and confidence interval for each Arrhenius parameter is shown in Table 2. The HPLC and modelling results are plotted in Figure 3 (A-F) and tabulated in supplementary information.

Table 1: Correlation of Fitting Parameters (refer to eq. 14-17 for P1:P4).

Fitting Parameter	P1	P2	P3	P4
P1	1.00000	0.77302	0.84918	0.33898
P2	0.77302	1.00000	0.49203	-0.31134
P3	0.84918	0.49203	1.00000	0.40687
P4	0.33898	-0.31134	0.40687	1.00000

Table 2: Arrhenius Parameters for CBZ Formation (1) and Cyanate Degradation.

Parameter	Value	95% Confidence Interval (Lower - Upper)	Units
A_1	$2.61 \cdot 10^7$	$2.29 \cdot 10^7$ - $2.98 \cdot 10^7$	L / (mol · s)
A_2	$6.56 \cdot 10^7$	$6.23 \cdot 10^7$ - $6.91 \cdot 10^7$	s^{-1}
EA_1	39.68	39.08 - 40.29	kJ / mol
EA_2	55.26	55.18 - 55.34	kJ / mol

The standard error of the selected parameters to the HPLC is 2.52 % of total reaction conversion, which corresponds to a 95% confidence interval of ± 4.94 % of total reaction conversion. The CBZ yield was defined as [moles of CBZ / (moles of CBZ + moles of ISB)] for each HPLC sample. The kinetic model with confidence intervals for each experiment is overlayed on the HPLC data in Figure 3.

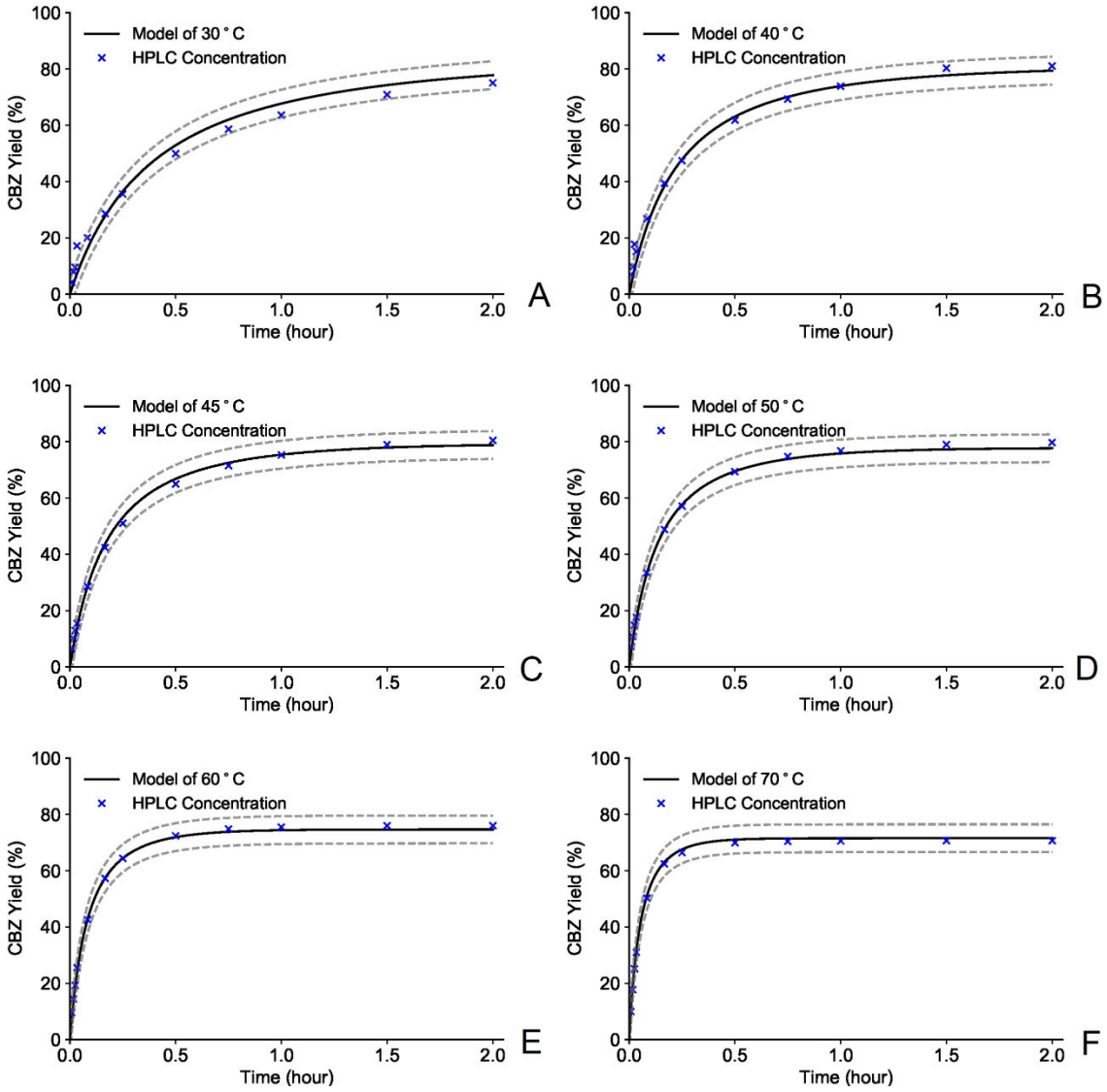

Figure 3: Formation of CBZ (% Yield) for batch reaction. HPLC measurements and fitted model predictions are shown. Reaction conditions were 1.1 eq. KOCN, 6 mg/mL ISB in acetic acid with 4% H_2O at 30 °C (A), 40 °C (B), 45 °C (C), 50 °C (D), 60 °C (E) and 70 °C (F). The dashed lines show the upper and lower confidence intervals of the kinetic model (± 4.94 %).

To elucidate the temperature effect, the kinetic model across all temperatures is plotted in Figure 4. Notably, as the reaction temperature increased, the initial reaction rate increased but the final in-solution yield decreased. According to the model, the final yield was lower at the higher temperatures due to the increased rate of cyanate degradation.

Only a slight excess of the cyanate reagent was utilized (1.1 mol. eq.) to elucidate the effects of the cyanate degradation. This experimental design permitted the simultaneous fitting of both pairs of Arrhenius parameters to the dataset. The developed kinetic reaction model helped in the selection of reaction conditions that maximize CBZ formation and minimize the cyanate degradation reaction for a continuous synthesis process.

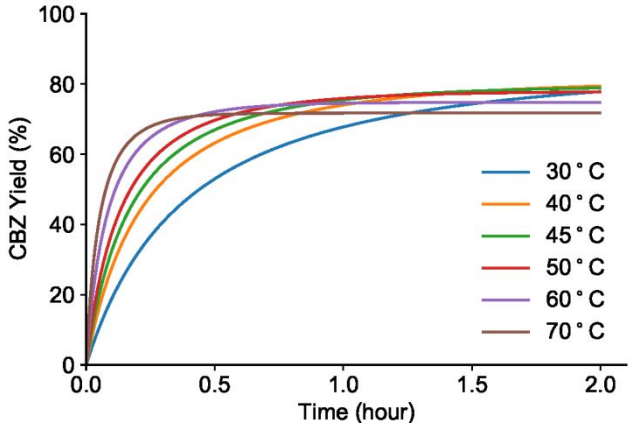

Figure 4: Plotted values for batch kinetic model prediction at 1.1 eq. KOCN, 6 mg/mL ISB in acetic acid with 4% H_2O.

In-line Raman Method Validation

A quantitative in-line Raman model to determine the CBZ and ISB concentrations within the ranges of the proposed continuous process was successfully developed and used for reaction monitoring during continuous synthesis of CBZ. The scripted Python baseline selection function proved advantageous in minimizing the interference between CBZ and ISB. The selected spectra regions of 707-738 cm^{-1} for CBZ and 1032-1057 cm^{-1} for ISB provided robust and repeatable correlation to concentration as determined by offline HPLC analysis. For each future calibration, these baselines were used. The limit of quantification and limit of detection for CBZ and ISB were calculated based on the residual error of the calibration curve according to ICH Q2 (R1) [24]. The results for the three validation days are reported in Table 3.

Table 3: In-line Raman method validation results for linearity, detection, and quantitation limits. Note: ppm = μg analyte/ mL solution.

Performance Metric	Calibration 1	Calibration 2	Calibration 3
ISB Correlation Coefficient (R^2)	0.9992	0.9996	0.9994
ISB Calibration Curve RMSE [ppm]	32	36	23
ISB Limit of Quantification [ppm]	261	149	198
ISB Limit of Detection [ppm]	78	45	59
ISB Slope [ppm / A.U]	2.66	2.62	2.64
ISB Intercept [ppm]	7.5	-43.9	-18
CBZ Correlation Coefficient (R^2)	0.9998	0.9998	0.9999
CBZ Calibration Curve RMSE [ppm]	77	47	42
CBZ Limit of Quantitation [ppm]	384	337	299
CBZ Limit of Detection [ppm]	115	101	90
CBZ Slope [ppm / A.U]	1.74	1.7	1.66
CBZ Intercept [ppm]	-59.4	-29.7	26.1

The correlation coefficient remained high across all periods (R^2 > 0.9992). The initial reproducibility of this method is reflected by the relatively small day to day changes in the slope and intercept of the calibration curve. The model was calibrated in the ranges of 0.25 - 2.50 mg/mL and 0.40 - 7.50 mg/mL for ISB and CBZ, respectively. The concentrations predicted outside of this range should be considered only semi-quantitative. During each validation period, a system suitability sample and three levels of quality controls were also assessed for accuracy and precision. The accuracy at each level was within the specifications (85-115)% and precision was less than 5% for all the quality control samples. It is hypothesized that the differences between the LOQ and LOD across the three calibration arms is a result of minor differences and sampling error in the preparation of the Raman and HPLC calibration curves. The variation of the Raman instrument background noise may also be a contributing factor.

During method validation, the accuracy and precision of the in-line Raman method was demonstrated for immediate use following a calibration curve prepared in the same analysis period. However, for practical use during CS experiments spanning over 7 days, it was necessary to assess the intermediate- reproducibility for the in-line Raman method over a 7-day period. Three bulk solutions of the quality control stocks were prepared, and the first aliquots were assessed the same day as a prepared calibration curve (Day 0). The stocks were then sealed and stored under refrigeration at 4 °C to avoid degradation/evaporation. For the following 7 days, additional aliquots of the quality control solutions were measured by in-line Raman and the concentration levels were assessed using the original Day 0 calibration curve. The refrigerated samples were tested by HPLC after each period of in-line Raman measurement throughout 7-day repeatability study. Within the 7-day period, the accuracy and precision of all quality control samples as measured by in-line Raman method remains well within the acceptable limits (85-115)% (Table S5). Therefore, the validity of using the calibration curve for up to seven days following the initial calibration was demonstrated.

Continuous Synthesis (CS) of CBZ

Kinetic modelling and simulation can be an effective tool to accelerate process development and provide insight into critical process parameters [6, 9, 16, 42]. In CS applications, it is critical to understand the relative impact of each process parameter on conversion and consequently product quality. For the CSTR process utilized in the current work, the concentration profile of the startup phase and equilibrium conversion was simulated and optimized for the batch CSTR process prior to continuous experimentation.

The simulation of the CSTR process helped to design and optimize the conditions for CS with reduced experimentation. The CSTR model was based entirely upon batch kinetics and was utilized to make determinations regarding the stochiometric equivalents of reagents and the temperature of operation. A 3-dimensional surface plot of the predicted equilibrium conversion was first generated using the batch CSTR experiments. In Figure 5, the simulation results of an ideal single stage CSTR with one-hour residence time are shown for varying equivalent of KOCN from 30 °C to 70 °C. The equilibrium conversion was approximated by extending the iterative solver for 40 residence times with a one second timestep. Although a single stage CSTR is demonstrated in this work, these equations could readily be applied to a multistage process to minimize KOCN equivalents and approach nearly complete conversion at the minimal cost. The limited effect of temperature on predicted conversion is demonstrated as well as the diminishing marginal benefit of increasing KOCN equivalents.

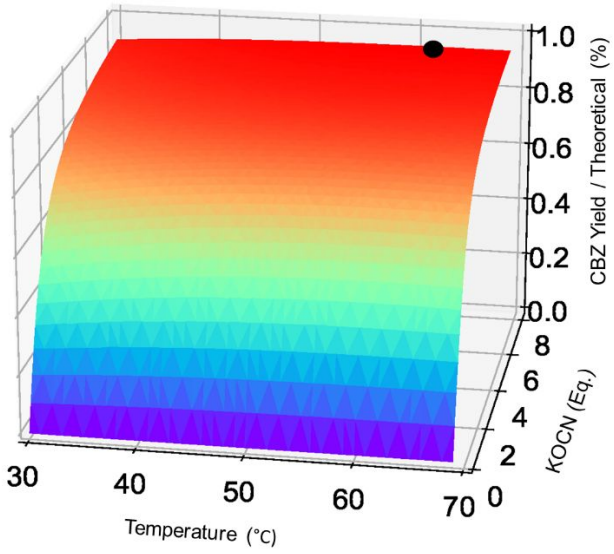

Figure 5 : Ideal CSTR model predicted equilibrium conversions for one hour residence time for the synthesis of CBZ starting from ISB and KOCN. The ISB stock is assumed at 6 mg/mL and the aqueous inlet phase is modelled at 4%

of the inlet overall volume. The maximum equivalents of KOCN (8.27 eq) corresponds to a nearly saturated KOCN aqueous phase (500 mg/mL) at the conditions described above.

For the dynamic equilibrium conversions within the simulated operating limits, the highest predicted equilibrium conversion shown on the surface plot, corresponding to 8.27 eq. KOCN at 61 °C, was 94.5% (7.04 mg/mL CBZ). These conditions, designated as the black dot, were considered the optimal case moving forward into the CS stage. Furthermore, each point on the surface plot corresponds to its own startup concentration profile. Modelling the concentration profile during the startup phase is helpful to predict when the product is within specifications—minimizing waste and maximizing efficiency.

The predicted optimal conditions were tested experimentally to demonstrate a high-yielding single-stage CSTR process. This CS experiment also served to simultaneously validate the CSTR kinetic model as well as the usefulness of in-line Raman method to determine dynamic quantitative levels of both CBZ and ISB from a multicomponent mixture. The kinetic model and experimental results are overlayed in Figure 6. HPLC timepoints are shown for comparison.

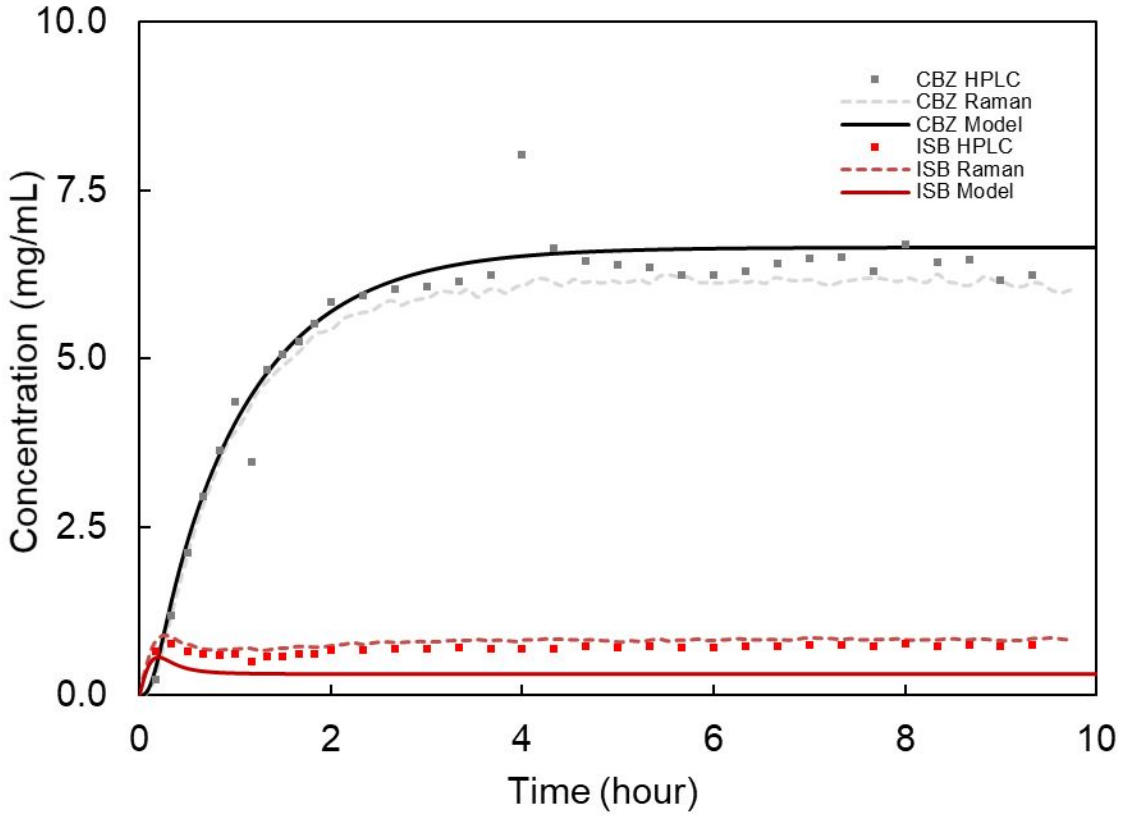

Figure 6: Startup of CSTR concentration profile by kinetic modelling, using in-line Raman, and offline HPLC analysis.

For the predicted optimal conditions, the kinetic model is a good fit to both the in-line Raman and the HPLC data. After 4 Residence times the average CBZ Yield (%) by HPLC was 87.9% compared to the model predicted conversion of 94.5%. This 6.6% deviation is slightly larger than the 95% confidence interval for the batch kinetic model (± 4.94 %). Based on experimental observations, it is suspected that the well-mixed model assumption may not be correct and may account for the residual error. The aqueous cyanate stream appeared to have some degree of immediate precipitation when first mixing of predominantly acetic acid with bulk CSTR phase. The precipitation of the cyanate could not be corrected by simply increasing the stirring rate. The actual concentration of the cyanate and consequently the CBZ yield was therefore lower than the model predicted value. Because the model overpredicted reaction conversion, the

ISB concentration was underpredicted. Furthermore, locally high concentrations of the cyanate during the initial mixing may have contributed to a faster degradation reaction. The CSTR kinetic model can largely be considered the theoretical limit of conversion for an ideal CSTR with respect to the confidence interval of the parameters.

Process Disturbances

Understanding the relative impact of the process input variables on reaction conversion and CBZ concentration is essential for the CS process. More so, it is necessary to analyze how quickly the product stream can return to the acceptable range following process disturbances. Disturbance modelling, coupled with the use of in-line PATs, is important in determining when product should be collected or diverted in a CM process [7, 10]. Product diversion is part of the control strategies for CM processes as per ICH Q13 and FDA CM Guidance. However, the experimental determination of process disturbance effects can be costly and time-consuming. Therefore, simulation is a useful tool for rapidly screening process dynamics. The iterative nature of the continuous kinetic model facilitates matrices input parameters—allowing for any process condition profile or combination thereof to be simulated. The concentration of reagents, flow rates, and temperatures are frequently considered as the critical control parameters (CPPs) for CS and were therefore the primary subject of this disturbance study [6, 9, 10]. In Figures 7-10 stepwise disturbances for four process parameters simulated are shown and the corresponding CSTR profile was predicted.

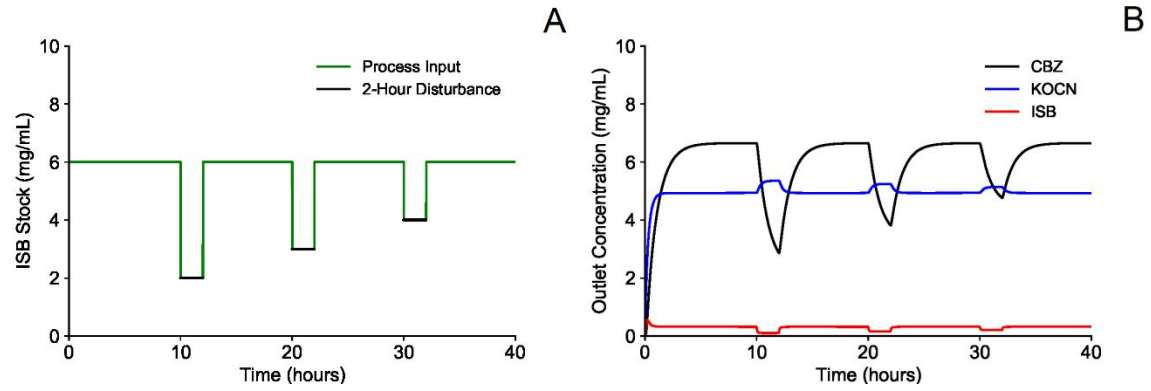

Figure 7: ISB stock concentration disturbance inlet (A) and outlet (B)

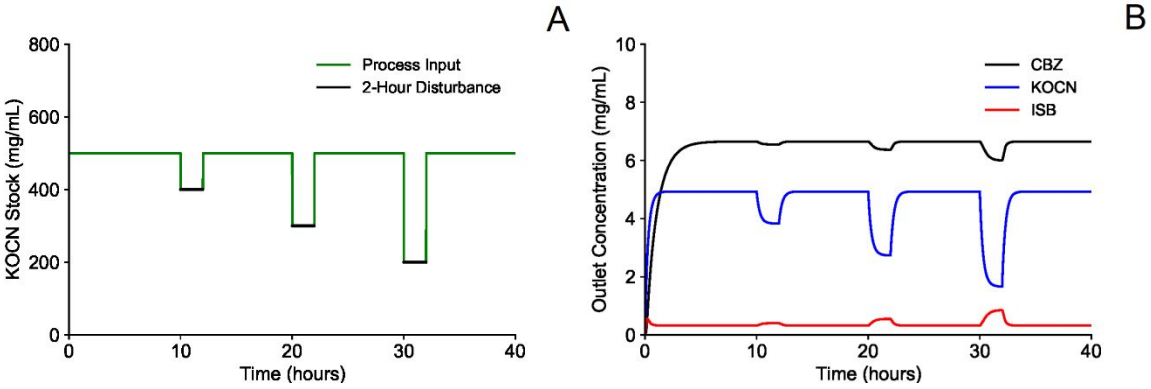

Figure 8: KOCN stock concentration disturbance inlet (A) and outlet (B)

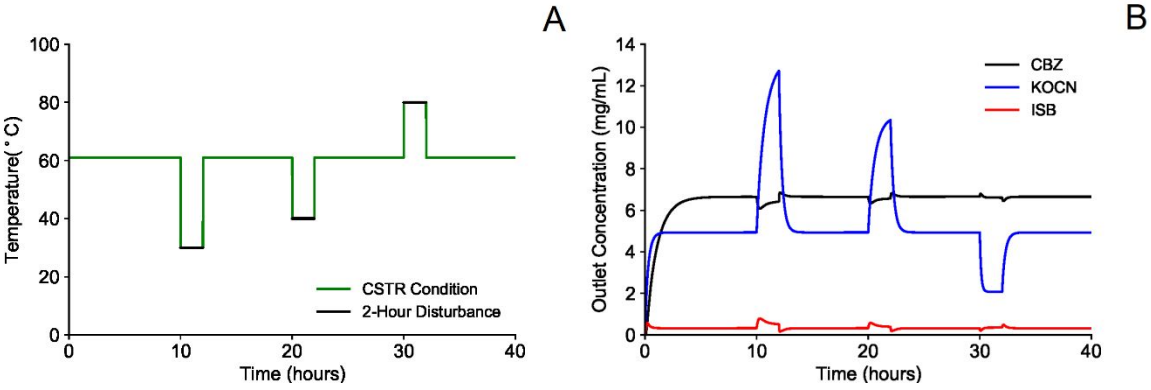

Figure 9: Temperature disturbance inlet (A) and outlet (B)

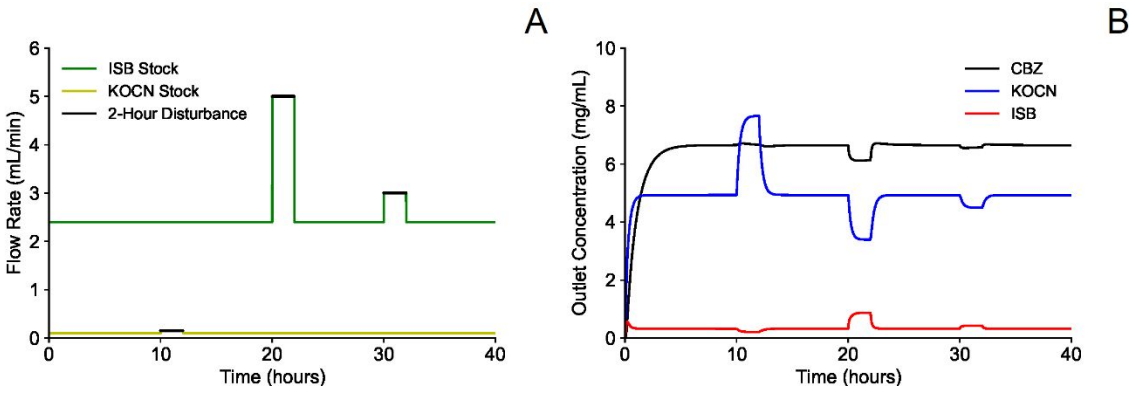

Figure 10: Flow rate disturbance inlet (A) and outlet (B).

Based on the simulation results, the ISB inlet concentration is the most critical process parameter (Figure 7). Because KOCN is in a large stoichiometric excess, the effects of changing inlet cyanate concentration are more limited compared to ISB (Figure 8). In Figure 10, the inlet concentration flow disturbances once again suggest that the outlet concentration profile is more dependent the limiting reagent ISB. The CSTR temperature (Figure 9) seemed to have the least effect on the CBZ and ISB concentration profiles of the simulated disturbance variables. Although at high temperatures the CBZ formation is more favorable, the rate of cyanate degradation is also increased resulting in less available cyanate for the CBZ reaction. Therefore, there is a more limited effect of temperature on conversion for the continuous process.

Two experimental disturbances were demonstrated as further validation for the continuous synthesis model. In the first verification experiment, a one-hour stepwise disturbance for the ISB inlet stock was conducted, and the concentration profile was monitored. The experimental results of in-line Raman and HPLC timepoints are overlayed on the kinetic model in Figure 11. Secondly, a one-hour stepwise disturbance in the KOCN concentration was conducted and is show in Figure 12.

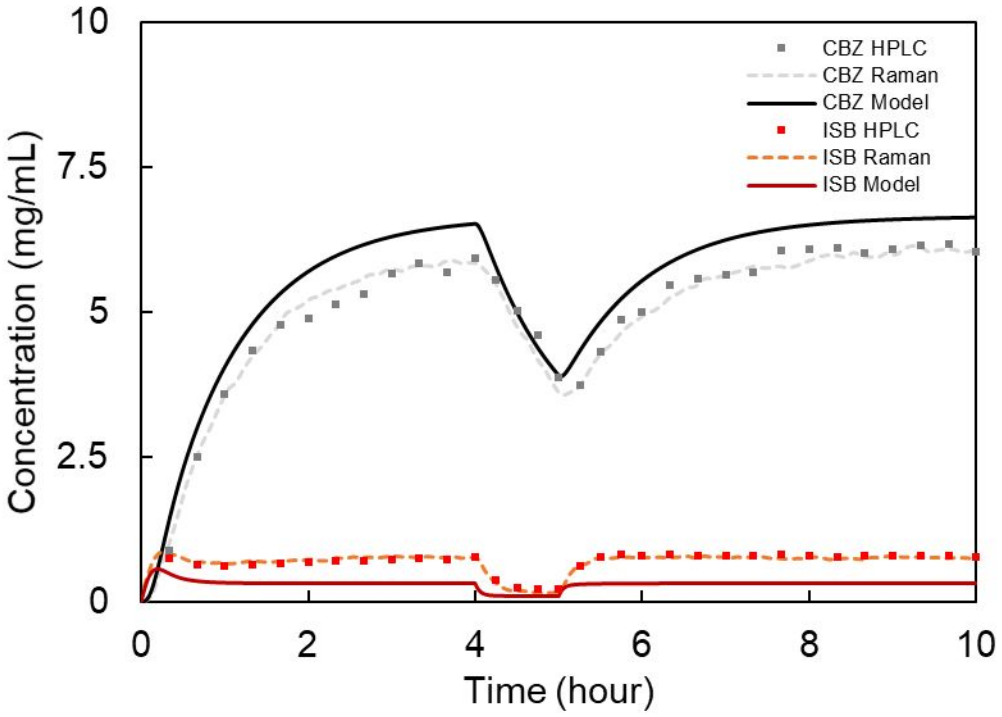

Figure 11: Experimental results for ISB stock concentration stepwise disturbance. The disturbance lasted from hour 4 to hour 5, ISB stock concentration was reduced from 6 mg/mL to 2 mg/mL.

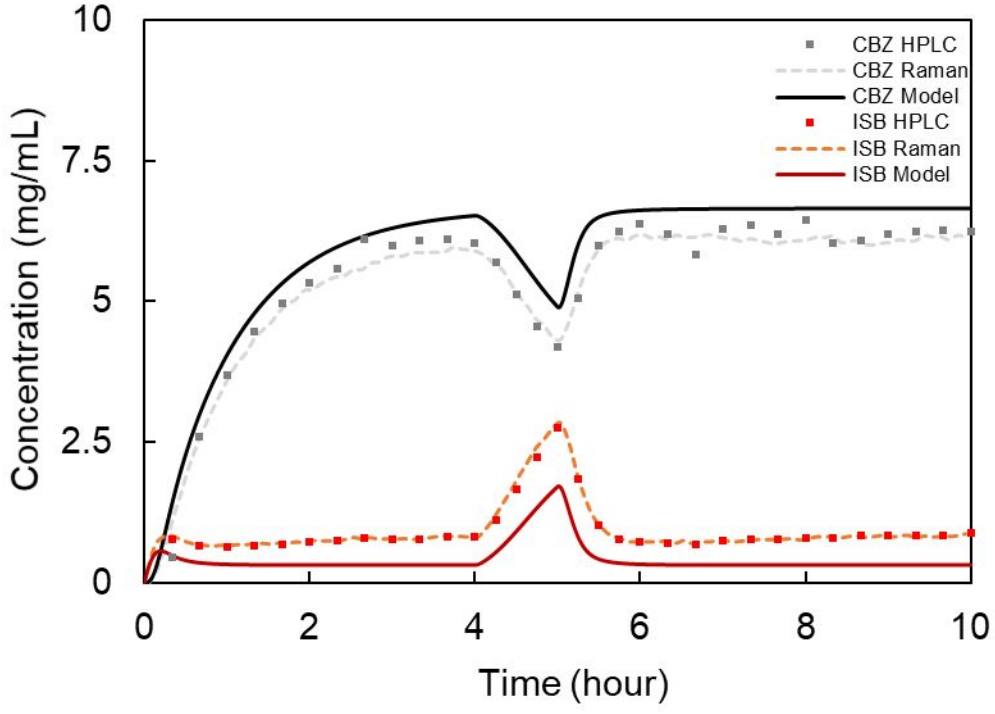

Figure 12: Experimental results for KOCN stock concentration stepwise disturbance. The disturbance lasted from hour 4 to hour 5, KOCN stock concentration was reduced from 500 mg/mL to 60 mg/mL.

For both disturbance experiments, the in-line Raman spectroscopy monitoring remained closely aligned to the HPLC timepoints. The experimental conversion remains slightly under the predicted value for the ideal CSTR kinetic model. Most importantly, it is demonstrated that the magnitude and duration of the product concentration changes for tested disturbances can be accurately simulated. The model is useful to predict the amount of time needed to return to the acceptable range of operation.

Conclusions

Kinetic parameters acquired during batch development were demonstrated as an effective tool for the design and optimization of a continuous synthesis process for CBZ. Process simulation studies aided in risk evaluation for different types, magnitudes, and durations of process disturbances. A validated in-line Raman spectroscopy method for the CS process was used to quantify and monitor both ISB and CBZ and help validate the process disturbance studies, leading to a high yielding, single stage CSTR process for continuous synthesis of CBZ.

Acknowledgement

This project was supported in part by an appointment to the Research Fellowship Program at the Office of Pharmaceutical Quality, Center for Drug Evaluation, U.S. Food and Drug Administration, administered by the Oak Ridge Institute for Science and Education through an interagency agreement between the U.S. Department of Energy and FDA.

References

1. Department of Human and Health Services, Food and Drug Administration, Guidance for Insdustry, 2004.
2. M. Baumann, T. S. Moody, M. Smyth and S. Wharry, *Org. Process Res. Dev.*, 2020, **24**, 1802-1813.
3. International Council of Harmonization, *ICH Q13 Guidance*, 2021.
4. M. Algorri, M. J. Abernathy, N. S. Cauchon, T. R. Christian, C. F. Lamm and C. M. V. Moore, *J Pharm Sci*, 2022, **111**, 593-607.
5. S. L. Lee, T. F. O'Connor, X. Yang, C. N. Cruz, S. Chatterjee, R. D. Madurawe, C. M. V. Moore, L. X. Yu and J. Woodcock, *J. Pharm. Innov.*, 2015, **10**, 191-199.
6. C. T. Armstrong, C. Q. Pritchard, D. W. Cook, M. Ibrahim, B. K. Desai, P. J. Whitham, B. J. Marquardt, Y. Chen, J. T. Zoueu, M. J. Bortner and T. D. Roper, *React Chem Eng*, 2019, **4**, 634-642.
7. K. P. Cole, J. M. Groh, M. D. Johnson, C. L. Burcham, B. M. Campbell, W. D. Diseroad, M. R. Heller, J. R. Howell, N. J. Kallman, T. M. Koenig, S. A. May, R. D. Miller, D. Mitchell, D. P. Myers, S. S. Myers, J. L. Phillips, C. S. Polster, T. D. White, J. Cashman, D. Hurley, R. Moylan, P. Sheehan, R. D. Spencer, K. Desmond, P. Desmond and O. Gowran, *Science*, 2017, **356**, 1144-1150.
8. M. V. Hernando, J. C. Moore, R. A. Howie, R. A. Castledine, S. L. Bourne, G. N. Jenkins, P. Licence, M. Poliakoff and M. W. George, *Org. Process Res. Dev.*, 2022, **26**, 1145-1151.
9. S. Diab, D. T. McQuade, F. B. Gupton and D. I. Gerogiorgis, *Org. Process Res. Dev.*, 2019, **23**, 320-333.
10. A. Mesbah, J. A. Paulson, R. Lakerveld and R. D. Braatz, *Org. Process Res. Dev.*, 2017, **21**, 844-854.
11. Y. Miyai, A. Formosa, C. T. Armstrong, B. Marquardt, L. Rogers and T. D. Roper, *Org. Process Res. Dev.*, 2021, **25**, 2707-2717.
12. V. K. Sthalam, A. K. Singh and S. Pabbaraja, *Org. Process Res. Dev.*, 2019, **23**, 1892-1899.
13. L. Rogers, N. Briggs, R. Achermann, A. Adamo, M. Azad, D. Brancazio, G. Capellades, G. Hammersmith, T. Hart, J. Imbrogno, L. P. Kelly, G. Liang, C. Neurohr, K. Rapp, M. G. Russell, C. Salz, D. A. Thomas, L. Weimann, T. F. Jamison, A. S. Myerson and K. F. Jensen, *Org. Process Res. Dev.*, 2020, **24**, 2183-2196.
14. N. S. Arden, A. C. Fisher, K. Tyner, L. X. Yu, S. L. Lee and M. Kopcha, *Int J Pharm*, 2021, **602**, 120554.
15. P. Sagmeister, R. Lebl, I. Castillo, J. Rehrl, J. Kruisz, M. Sipek, M. Horn, S. Sacher, D. Cantillo, J. D. Williams and C. O. Kappe, *Angew Chem Int Ed Engl*, 2021, **60**, 8139-8148.
16. E. Içten, A. J. Maloney, M. G. Beaver, D. E. Shen, X. Zhu, L. R. Graham, J. A. Robinson, S. Huggins, A. Allian, R. Hart, S. D. Walker, P. Rolandi and R. D. Braatz, *Org. Process Res. Dev.*, 2020, **24**, 1861-1875.
17. J. Deng, S. Staufenbiel and R. Bodmeier, *Eur J Pharm Sci*, 2017, **105**, 64-70.
18. J. Ouyang, J. Chen, I. Rosbottom, W. Chen, M. Guo and J. Y. Y. Heng, *CrystEngComm*, 2021, **23**, 813-823.
19. L. E. McMahon, P. Timmins, A. C. Williams and P. York, *J Pharm Sci*, 1996, **85**, 1064-1069.
20. D. Acevedo, X. Yang, A. Mohammad, N. Pavurala, W. L. Wu, T. F. O'Connor, Z. K. Nagy and C. N. Cruz, *Org. Process Res. Dev.*, 2018, **22**, 156-165.
21. X. Yang, D. Acevedo, A. Mohammad, N. Pavurala, H. Wu, A. L. Brayton, R. A. Shaw, M. J. Goldman, F. He, S. Li, R. J. Fisher, T. F. O'Connor and C. N. Cruz, *Org. Process Res. Dev.*, 2017, **21**, 1021-1033.

22. D. Acevedo, W. L. Wu, X. Yang, N. Pavurala, A. Mohammad and T. F. O'Connor, *CrystEngComm*, 2021, **23**, 972-985.
23. H. F. Kraus, D. Acevedo, W. Wu, T. F. O'Connor, A. Mohammad and D. Liu, *Reaction Chemistry & Engineering*, 2023, DOI: 10.1039/d2re00409g.
24. International Council of Harmonization, *ICH Q2(R1)*, 1996.
25. USP 1225, *Natl. Forum*, 2017, **38**.
26. USP 621, *Natl. Forum*, 2017, **38**.
27. W. M. Lister, *Can. J. Chem.*, 1954, **33**.
28. L. Tiwari, V. Kumar, B. Kumar and D. Mahajan, *RSC Advances*, 2018, **8**, 21585-21595.
29. G. Van Rossum, and Drake Jr, F. L. , *Centrum voor Wiskunde en Informatica Amsterdam*, 1995.
30. C. R. Harris, K. J. Millman, S. J. van der Walt, R. Gommers, P. Virtanen, D. Cournapeau, E. Wieser, J. Taylor, S. Berg, N. J. Smith, R. Kern, M. Picus, S. Hoyer, M. H. van Kerkwijk, M. Brett, A. Haldane, J. F. Del Rio, M. Wiebe, P. Peterson, P. Gerard-Marchant, K. Sheppard, T. Reddy, W. Weckesser, H. Abbasi, C. Gohlke and T. E. Oliphant, *Nature*, 2020, **585**, 357-362.
31. Pandas-Development-Team, 2020, **doi.org/10.5281/zenodo.3509134**.
32. P. Virtanen, R. Gommers, T. E. Oliphant, M. Haberland, T. Reddy, D. Cournapeau, E. Burovski, P. Peterson, W. Weckesser, J. Bright, S. J. van der Walt, M. Brett, J. Wilson, K. J. Millman, N. Mayorov, A. R. J. Nelson, E. Jones, R. Kern, E. Larson, C. J. Carey, I. Polat, Y. Feng, E. W. Moore, J. VanderPlas, D. Laxalde, J. Perktold, R. Cimrman, I. Henriksen, E. A. Quintero, C. R. Harris, A. M. Archibald, A. H. Ribeiro, F. Pedregosa, P. van Mulbregt and C. SciPy, *Nat Methods*, 2020, **17**, 261-272.
33. J. D. Hunter, *Comput Sci Eng.*, 2007, **3**, 90-95.
34. D. Gutman and W. Baidossi, *International Patent*, 2003, **WO 03/106414 A2**.
35. N. Karusala, S. Tummalapally, A. Talatala and D. Datta, *US Patent*, 2013, **8,530,647 B2**.
36. N. R. Karusala, U. S. Tummalapalaly and A. Talatala, *International Patent*, 2009, **WO 2009/139001 A2**.
37. R. Eckardt and H. Jansch, *US Patent*, 2006, **7,015,322 B1**.
38. A. Milanese, *US Patent*, 1998, **5,808,058**.
39. B. Ravinder, S. Rajeshwar Reddy, M. Sridhar, M. Murali Mohan, K. Srinivas, A. Panasa Reddy and R. Bandichhor, *Tetrahedron Lett.*, 2013, **54**, 2841-2844.
40. S. A. Ansari, R. Bhat and A. K. Kulkarni, *EP 1 302 464 A1*, 2003.
41. K. D. Vyas, W. S. Jafri and A. K. Kulkarni, *US Patent*, 2001, **6,245,908 BI**.
42. H. G. Jolliffe and D. I. Gerogiorgis, *ChERD*, 2015, **97**, 175-191.